



LJMU Research Online

Webb, SD, Reddyhoff, D, Ward, J, Williams, D and Regan, S

Timescale analysis of a mathematical model of acetaminophen metabolism and toxicity

<http://researchonline.ljmu.ac.uk/id/eprint/2164/>

Article

Citation (please note it is advisable to refer to the publisher's version if you intend to cite from this work)

Webb, SD, Reddyhoff, D, Ward, J, Williams, D and Regan, S (2015) Timescale analysis of a mathematical model of acetaminophen metabolism and toxicity. Journal of Theoretical Biology, 386. pp. 132-146. ISSN 1095-8541

LJMU has developed **LJMU Research Online** for users to access the research output of the University more effectively. Copyright © and Moral Rights for the papers on this site are retained by the individual authors and/or other copyright owners. Users may download and/or print one copy of any article(s) in LJMU Research Online to facilitate their private study or for non-commercial research. You may not engage in further distribution of the material or use it for any profit-making activities or any commercial gain.

The version presented here may differ from the published version or from the version of the record. Please see the repository URL above for details on accessing the published version and note that access may require a subscription.

For more information please contact researchonline@ljmu.ac.uk

<http://researchonline.ljmu.ac.uk/>

Timescale analysis of a mathematical model of Acetaminophen metabolism and toxicity.

Dennis Reddyhoff^{a,*}, John Ward^a, Dominic Williams^b, Sophie Regan^c,
Steven Webb^c

^a*Department of Mathematical Sciences, Loughborough University, Loughborough, Leics,
LE11 3TU, UK.*

^b*Translational Safety, Drug Safety and Metabolism, Darwin Building, Cambridge Science
Park, Milton Road, Cambridge, Cambs, CB4 0FZ, UK.*

^c*MRC Centre for Drug Safety Science, Dept. of Molecular and Clinical Pharmacology,
Institute of Translational Medicine, University of Liverpool Sherrington Building, Ashton
Street, Liverpool, L69 3GE, UK*

Abstract

Acetaminophen is a widespread and commonly used painkiller all over the world. However, it can cause liver damage when taken in large doses or at repeated chronic doses. Current models of acetaminophen metabolism are complex, and limited to numerical investigation though provide results that represent clinical investigation well. We derive a mathematical model based on mass action laws aimed at capturing the main dynamics of acetaminophen metabolism, in particular the contrast between normal and overdose cases, whilst remaining simple enough for detailed mathematical analysis that can identify key parameters and quantify their role in liver toxicity. We use singular perturbation analysis to separate the different timescales describing

*Corresponding Author

Email address: d.reddyhoff@lboro.ac.uk (Dennis Reddyhoff)

the sequence of events in acetaminophen metabolism, systematically identifying which parameters dominate during each of the successive stages. Using this approach we determined, in terms of the model parameters, the critical dose between safe and overdose cases, timescales for exhaustion and regeneration of important cofactors for acetaminophen metabolism and total toxin accumulation as a fraction of initial dose.

Keywords: Acetaminophen, modelling, analysis, metabolism, toxicology.

1. Introduction

Acetaminophen (paracetamol; APAP *N-acetyl p-aminophenol*) is a commonly used pain killer and antipyretic. It is an easy to obtain medication that is nowadays widely stocked in pharmacies and corner shops, in packets of up to 32 tablets (16 in Europe); enough to cause serious liver damage if ingested in a single dose. It is estimated that in the U.S. an average of 56000 people are admitted to the hospital each year due to acetaminophen overdoses and their related effects. Over 450 people a year go on to die from acetaminophen overdose. In the U.S. alone, adverse drug reactions are ranked as being between the 4th and 6th leading cause of death [1]. Worryingly, around a quarter of these deaths are not from an intentional overdose by way of a suicide attempt, but from chronic use of the drug. The number of deaths associated with acetaminophen overdose in the U.S. almost doubled over a 4 year period, from 98 deaths in 1997 to 173 deaths in 2001 [2]. In the UK, 90 to 155 people died per year between 2000 and 2008 with additional

16 deaths due to acetaminophen being taken with other drugs [3]. This ease
17 of availability and lack of awareness of its potential hazards means that ac-
18 etaminophen is responsible for 80% of drug-associated cases of liver injury [4],
19 and drug-induced liver injury has become the most common cause of acute
20 liver failure and subsequently transplantation in Western countries [5]. Much
21 of our understanding of the metabolism and toxicology of APAP comes from
22 animal models, particularly rat and mouse. Interestingly there is consider-
23 able variation in toxicity between species [6].

24 APAP is taken orally and is absorbed into the blood stream. It arrives in
25 the liver via the hepatic portal vein and moves through the liver mass to the
26 central vein (Figure 1). In this time, APAP is absorbed into the hepatocytes
27 where it is metabolised. In the liver, hepatocyte function is determined by
28 position relative to the portal vein, with functions differing if a hepatocyte is
29 near the blood inlet (periportal) or outlet (centrilobular), an affect known as
30 zonation and is present across all areas of the liver [7]. APAP is metabolised
31 in the liver primarily by the sulphation and glucuronidation pathways [8, 9],
32 while around 5% is metabolised, via oxidation, to form the toxic metabolite
33 *N*-acetyl *p*-benzoquinone imine (NAPQI) [10]. A detailed pathway diagram is
34 shown in Figure 2 and a simplified one used as the basis for the mathematical
35 modelling is shown in Figure 3. The sulphation pathway involves the conju-
36 gation of APAP with the cosubstrate 3'-phosphoadenosine 5'-phosphosulfate
37 or PAPS. This cosubstrate is finite within the liver cell and at toxic doses we
38 see PAPS levels fall [11] and a saturation of the sulphation pathway, leading

39 to higher metabolism through glucuronidation and oxidation. The cofactors
40 associated with the glucuronidation pathway have a much higher capacity
41 than those of the sulphation pathway [12] and we assumed in our modelling
42 that the pathway does not saturate at clinically relevant, high APAP doses.
43 Via the oxidation pathway, APAP is catalysed by select enzymes from a ‘su-
44 perfamily’ of enzymes known as Cytochrome P450 [13]. The main enzymes
45 involved in this reaction in human cells are Cytochromes CYP2E1,CYP3A4
46 and CYP1A2 [13, 14, 15], however, the sub-type and hence nomenclature of
47 the enzymes varies by species when looking at animal models. Metabolism
48 through oxidation produces NAPQI, a chemically reactive and toxic metabo-
49 lite. NAPQI can be detoxified by GSH, an antioxidant which conjugates to
50 NAPQI preventing binding with essential proteins and thus preventing dam-
51 age to the liver. At sufficiently high doses, the sulphation cosubstrate, PAPS,
52 can be exhausted, diverting quantitatively more APAP through the oxida-
53 tion pathway, leading to higher amounts of NAPQI being produced. There
54 are marked species differences in the sensitivity to APAP, e.g. rats are re-
55 sistant to equivalent doses of APAP compared with humans, and this is due
56 to a much greater capacity for sulphation and a lowered propensity for ox-
57 idation [16]. Oxidation has the effect of depleting GSH levels in the liver,
58 through binding with NAPQI and hence greater levels of protein adducts
59 are produced. GSH can also be depleted by individual factors such as alco-
60 holism [17] and anorexia [18] though this inter-patient variability is beyond
61 the scope of the mathematical model to be presented in this paper.

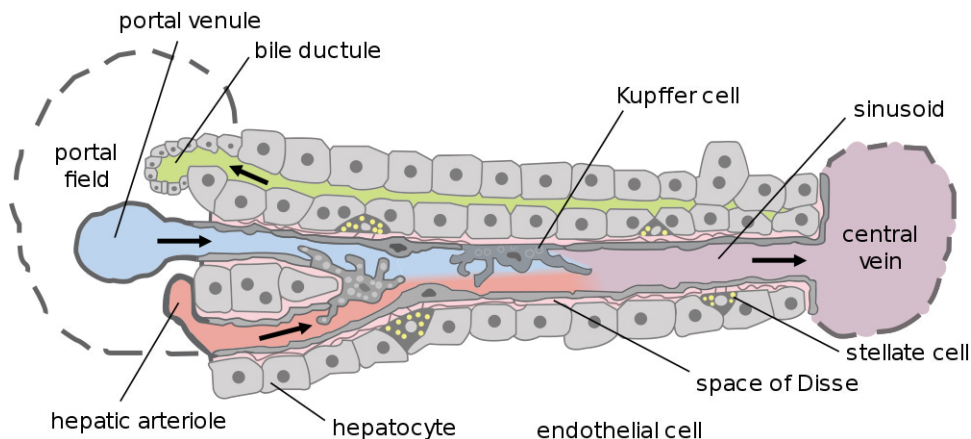


Figure 1: **Structure of the liver** [36]. Blood flows from the portal field (left) to the central vein. APAP in the blood diffuses into the hepatocytes and is metabolised.

62 It is broadly recognised that mathematical modelling now plays a signifi-
 63 cant part in the drug development process. A successful model provides a cost
 64 effective way of understanding and predicting drug efficacy and toxicology,
 65 thus offering a systematic means of guiding more focused, less exploratory,
 66 use of animal models. Despite acetaminophen being the subject of labora-
 67 tory studies for many years, it is only recently that theoretical studies on
 68 the toxicology of paracetamol have been undertaken. One of the first math-
 69 ematical models produced is by Reith *et al.* [12], who focused on examining
 70 the kinetics of the glucuronidation and sulphation pathways using a 14 vari-
 71 able ordinary differential equation (ODE) model and fitting to human data,
 72 specifically excreted products in the plasma. Ochoa *et al.* [19] took a mul-
 73 tiscala approach, combining a detailed cell based APAP metabolism model,
 74 comprised of 34 variables, with a whole body model to simulate actions in
 75 the liver and transport between organs. Both these models are rich in detail

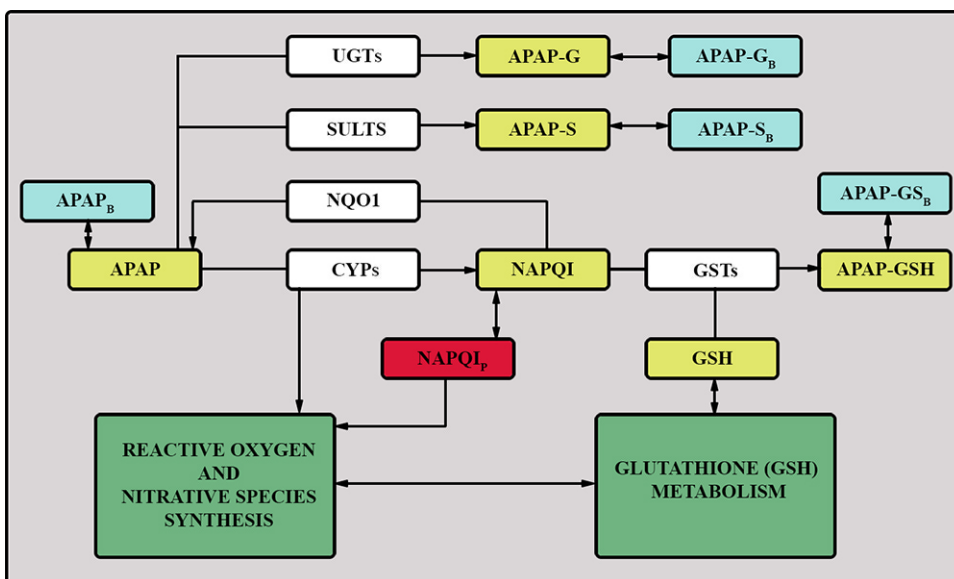


Figure 2: **A diagram of the cell scale metabolic network for APAP metabolism.** The abbreviations are: APAP, acetaminophen; UGTs, UDP-glucuronosyltransferases; SULTs, sulfotransferase; NQO1, NADPH-quinoreductase; CYPs, cytochrome P450; APAP-G, acetaminophen glucuronide; APAP-S, acetaminophen sulphate; NAPQI, N-acetyl-p-benzoquinone imine; GSTs, glutathione S-transferase; GSH, glutathione; APAP-GSH, acetaminophen glutathione conjugate. Subscript 'B' denotes non-specific binding to a protein or lipid. Subscript 'P' denotes binding to non-specific protein [19]. Blue boxes are non specifically bound products, yellow boxes are molecules, white boxes are isozymes, red boxes are protein bound molecules and green boxes are further metabolic systems not described in this diagram.

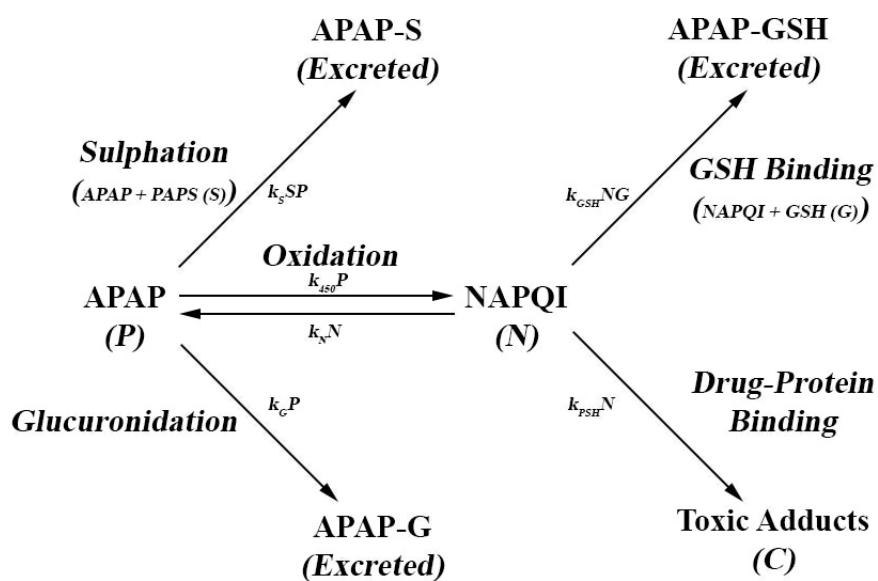


Figure 3: **Pathway Diagram for APAP Metabolism.** APAP is metabolised through 3 main pathways, sulphation, glucuronidation and oxidation. CYP oxidation creates NAPQI, a harmful metabolite which can bind with essential cellular proteins within the hepatocytes if no GSH is present. Modelled species are APAP (P), NAPQI (N), PAPS (S), GSH (G) and Drug-Protein Adducts (C).

76 and parameter estimation, but their complexity prohibits investigation using
77 more advanced mathematical techniques. Multi-compartmental models have
78 also been tested by Ben-Shachar *et al.* [20] who looked to create a model
79 that would reproduce clinical and experimental data on APAP and metabo-
80 lite levels in the plasma and urine. They looked to reproduce the data of
81 Prescott *et al.* [21] examining APAP metabolism in human patients. Again,
82 this model is complex and so it is difficult to apply mathematical analysis.
83 Remien *et al.* [22] investigate a simple model for APAP metabolism, utilis-
84 ing a tissue-scale model to predict biomarker levels, which can be used to
85 estimate overdose amount, time elapsed since overdose, and likelihood of pa-
86 tient survival. In this paper we will present a cell-based model that describes
87 the major pathways in the system, which is more detailed then the model
88 proposed by Remien *et. al* but very much simpler than that of Reith and
89 Ochoa *et al.* [12, 19]. This model will in fact be applicable to a broad range
90 of drugs that are metabolised in the liver via (1) a non exhaustible pathway
91 (i.e. glucuronidation), (2) an exhaustible pathway (i.e. sulphation) and (3)
92 an oxidation pathway that leads to GSH binding and toxic conjugate for-
93 mation. The resulting model is amenable to two forms of analysis. Firstly,
94 to identify which parameters have the most affect on the predicted outcome
95 through sensitivity analysis and, secondly, to derive relatively simple for-
96 mula, using singular perturbation analysis, for factors such as critical initial
97 dose and timescales for peak toxic activity. This will enable us to probe the
98 model to gain great insight in to how individual mechanisms in the model

99 can affect and influence these factors. Though the focus will be on APAP
100 metabolism in humans, the modelling and analysis is applicable preclinical
101 animal models also.

102 We seek to create a model that captures the most important aspects
103 of APAP metabolism and toxicity at the cellular level. We then analyse
104 the model both numerically and analytically in order to develop a better
105 understanding of the interactions in the modelled system. We also wish to
106 identify any data gaps which can then be pursued experimentally. In the
107 next section we will derive the model. In Section 3.1 we present simulations,
108 showing the metabolic responses to bolus doses of APAP and undertake
109 parameter sensitivity analysis. In Section 4 we perform a detailed timescale
110 analysis, to derive formula characterising APAP metabolism. Finally we
111 summarise the key results and discuss future work in Section 5.

112 **2. Mathematical Modelling**

113 *Model Background.*

114 We focus on the metabolism of paracetamol within a single hepatocyte,
115 aiming to capture the main dynamics of APAP metabolism while maintaining
116 enough simplicity that analytical progress is possible. The full metabolic
117 process is summarised in Figure 2 and, as stated before, broadly separates
118 into three pathways. Describing all of the pathways illustrated in Figure 2
119 would lead to an extremely complex model involving 20+ state variables and
120 many more parameters. Instead, as a first approximation, we bundle all the

121 pathways in the glucuronidation route into a single pathway and likewise
 122 for sulphation and oxidation. The reduced pathway diagram used for the
 123 model is shown in Figure 3. We assume for sulphation and glucuronidation
 124 that the first reaction down each pathway is non-, or negligibly, reversible, so
 125 that events downstream do not directly affect paracetamol metabolism. For
 126 the oxidation pathway, we assume a single generic CYP is involved which
 127 represents the combined actions of CYP2E1, CYP3A4 and CYP1A2.

128 *Model Description.*

129 We use mass action laws to derive a system of ordinary differential equa-
 130 tions that describe the dynamics over time of the different pathways illus-
 131 trated in Figure 3. The resulting model is the same as that presented, but not
 132 studied, in Williams *et al.* [23], we will nevertheless outline the model deriva-
 133 tion. The model variables are listed in Table 1 and we note they represent
 quantities per cell.

Table 1: **Model variables and their units.**

Variable	Interpretation	Units
P	Paracetamol (APAP)	mol/cell
S	Sulphate (PAPS)	mol/cell
N	NAPQI	mol/cell
G	GSH	mol/cell
C	Protein Adducts	mol/cell

134

135 Our model assumes an initial bolus dose being delivered. The metabolism
 136 depends on the size of the initial dose. At regular doses the majority of APAP

137 will be metabolised by the sulphation and glucuronidation pathways [10].
138 APAP (P) undergoes sulphation by reacting with the PAPS enzyme (S) at
139 rate $k_S SP$, where k_S is the rate constant associated with the metabolism
140 of APAP by PAPS, ultimately forming APAP-S. In humans, PAPS is ex-
141 haustible and so at high doses may, in some situations, see a saturation of
142 the pathway. We define the rate constant for the production of PAPS by the
143 liver as b_S and the rate constant for the natural decay as d_S . In contrast,
144 we assume that the enzymes involved in glucuronidation are not exhaustible
145 and are present at an approximately constant concentration, hence APAP
146 metabolism along this pathway is in affect a natural decay at rate $k_G P$.

147 The remaining APAP is metabolised via the oxidation pathway creat-
148 ing NAPQI (N). We assume that cytochrome P450 enzymes are present
149 continuously at an approximately fixed concentration, so that the oxidative
150 pathway is described as a further “natural decay” term, $k_{450} P$. This reaction
151 is assumed reversible at rate $k_N N$.

152 NAPQI is assumed to be metabolised via one of two pathways. The first
153 is by reaction with the antioxidant GSH (G) at a rate $k_{GSH} NG$. At normal
154 doses of APAP we expect to see nearly all of the NAPQI produced being
155 detoxified by this pathway. Conjugation with GSH renders NAPQI harmless
156 and it is excreted from the body with no ill effects. In our model GSH is
157 assumed to be constitutively produced at a constant rate b_G and naturally de-
158 cays at rate $d_G G$. In fact, the production and regulation of GSH production
159 is quite complex, being released from skeletal muscle [24] and regulated as an

160 adaptive mechanism by NRF2 [25]; at the level of detail of the current model
 161 we assume that constant b_G is a reasonable starting point for modelling single
 162 doses. The second pathway has NAPQI creating drug-protein adducts (C)
 163 at a rate $k_{PSH}N$. This binding to cellular macromolecules can result in cell
 164 death if the proteins that are bound are essential for cell function/viability.
 165 We do not consider the downstream events caused by drug-protein adducts
 166 and the variable C represents the total accumulated amount of a toxic re-
 167 action (we therefore hereon refer to C as toxins in that they are capable of
 168 inducing cell death).

We arrive at the following model describing the pathways in Figure 3 and including the stated assumptions;

$$\frac{dP}{dt} = -k_S SP - k_G P - k_{450} P + k_N N, \quad (1)$$

$$\frac{dS}{dt} = -k_S SP + b_S - d_S S, \quad (2)$$

$$\frac{dN}{dt} = k_{450} P - k_N N - k_{GSH} NG - k_{PSH} N, \quad (3)$$

$$\frac{dG}{dt} = -k_{GSH} NG + b_G - d_G G, \quad (4)$$

$$\frac{dC}{dt} = k_{PSH} N. \quad (5)$$

169

170

171 We assume in this study that the drug is introduced into cells as a single bolus
 172 dose at $t = 0$ at a concentration P_S . The cells at this point are assumed to

173 be at pretreatment steady-state level. The initial conditions for this system
174 are thus

$$P(0) = P_S, \quad S(0) = \frac{b_S}{d_S}, \quad G(0) = \frac{b_G}{d_G}, \quad N_0 = 0, \quad C(0) = 0. \quad (6)$$

175 Table 2 lists the model parameters and their estimated values for the
176 standard simulation. Where possible, we obtained their values from the lit-
177 erature and any remaining parameters through repeated simulation, so that
178 the numerical results matched reasonably well with similar simulations from
179 Remien *et al.* [22]. It is generally considered that anything more than 4g
180 taken at once is considered an overdose, so we use 4g as our safe dose case [26]
181 (though it is recommended to take no more than a 1g dose at 4 hour intervals).

182

183 3. Results

184 3.1. Simulation

185 Our aim is to understand the effect of dose on both NAPQI produc-
186 tion and timescales of events in APAP metabolism. We solve the system
187 of equations (1) - (5) using the MATLAB routine ode15s, a variable order
188 backwards difference method. Unless otherwise stated, we use the parameter
189 values listed in Table 2.

190 We first examine the single 4g dose case, i.e. a daily dose in a single

Table 2: List of model parameters and values used in standard simulation

Parameter	Value	Units	Notes
P_0	1.32×10^{-13}	$\text{mol} \cdot \text{cell}^{-1}$	See (1)
d_G	2	day^{-1}	[27, 28, 29]
b_G	1.374×10^{-14}	$\text{mol} \cdot \text{cell}^{-1} \cdot \text{day}^{-1}$	[22]
k_{GSH}	1.6×10^{18}	$\text{cell} \cdot \text{mol}^{-1} \cdot \text{day}^{-1}$	[30]
k_G	2.99	day^{-1}	[12]
$k_S^{[*]}$	2.26×10^{14}	$\text{cell} \cdot \text{mol}^{-1} \cdot \text{day}^{-1}$	See (2)
$b_S^{[*]}$	2.65×10^{-14}	$\text{mol} \cdot \text{cell}^{-1} \cdot \text{day}^{-1}$	See (2)
$d_S^{[*]}$	2	day^{-1}	Equal to d_G
$k_{450}^{[*]}$	0.315	day^{-1}	See (3)
$k_N^{[*]}$	0.0315	day^{-1}	See (4)
$k_{PSH}^{[*]}$	110	day^{-1}	See (5)

- (1) 4g dosage, standard single dose assuming 80% of dose reaches liver.
- (2) Assuming initial PAPS is 10% of standard APAP dose i.e. $\frac{b_S}{d_S} = \frac{P_0}{10}$, and initially sulphation and glucuronidation are about the same, i.e. $k_S = \frac{k_G d_S}{b_S}$ i.e. amounts to 47.5% of APAP processing initially.
- (3) Equal to $\frac{k_G}{9.5}$ i.e. we assumed only 5% of APAP is oxidised initially.
- (4) Assumed $k_N = \frac{k_{450}}{10}$ i.e. forward reaction is dominant.
- (5) Assuming at normal GSH concentration, $\frac{b_G}{d_G}$, only 1% of NAPQI binds with the hepatocytes, i.e. $k_{PSH} = 0.01 \frac{k_{GSH} b_G}{d_G}$.

Parameters marked with ^[*] indicate parameters chosen by us to produce physiologically realistic results.

191 bolus. We expect GSH levels to remain non-negligible to ensure a safe low-
 192 level conjugation of NAPQI. Consequently, protein adducts will then stay at
 193 very low levels. Both of these features can be observed from the simulation
 194 in Figure 4 (left column).

195 It can be seen that neither GSH or Sulphation levels drop to zero, indi-
 196 cating that all APAP in the system is being dealt with effectively. We do

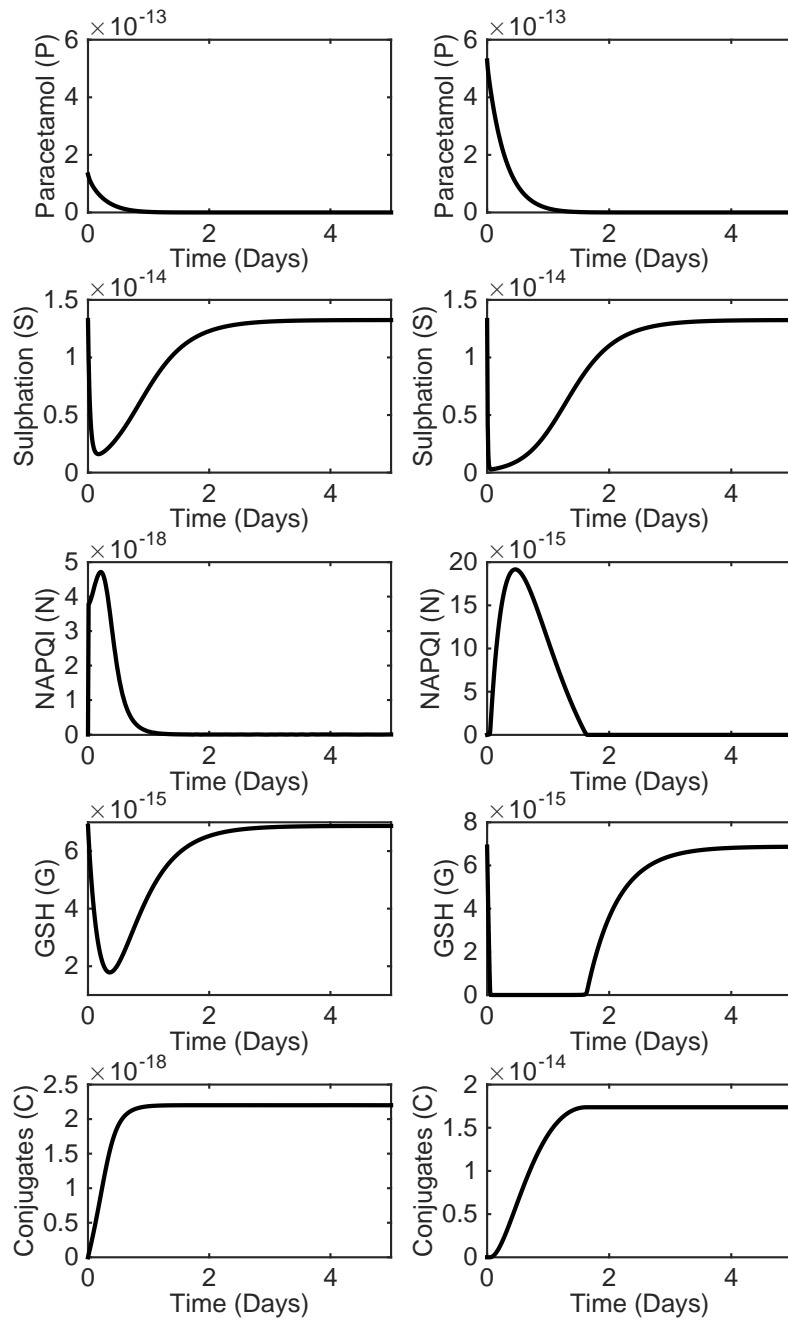


Figure 4: **Plot of the evolution of, from top to bottom, APAP, PAPS, NAPQI, GSH and protein adducts respectively.** The units in each graph are mol/cell, noting the two orders of magnitude difference between the levels in N and C . Here 4g (left) and 16g (right) correspond to $P_0 = 1.32 \times 10^{-13}$ and $P_0 = 5.28 \times 10^{-13}$ mol/cell, respectively.

197 see a rise in NAPQI, however overall levels are extremely low relative to our
198 overdose case and therefore do not pose any great risk. The same can be
199 observed for the protein adducts, which remain at low levels compared to
200 the overdose case.

201 For the overdose case of 16g, a likely outcome is that both GSH and sul-
202 phate levels will become exhausted at some stage of the metabolism process.
203 This indeed occurs as can be seen in Figure 4 (right column). Sulphates drop
204 very rapidly to a near zero level and take a long time to recover; this means
205 that proportionally more APAP will be conjugated into NAPQI. This leads
206 to a rapid drop in GSH to negligible levels that are sustained for a period
207 of about 40 hours. This rise in NAPQI and subsequent depletion of GSH
208 results in a high level of formation of protein adducts in comparison with our
209 safe dose simulation. We note that a 4x increase in dose leads to an almost
210 $10^4 \times$ increase in accumulated protein adducts.

211 Figure 5 shows the affect of the initial dose on the total amounts of toxic
212 protein adducts produced, presented as C_∞/P_S , where C_∞ represents the
213 steady state level i.e. $C \rightarrow C_\infty$ as $t \rightarrow \infty$ and the ratio C_∞/P_S represents
214 the fraction of adduct molecules produced per APAP molecule. At levels just
215 slightly above a safe dose of 4g it can be seen that the amount of protein
216 adducts in the system rises rapidly. This rapid increase in protein conjugate
217 formation displays how dangerous overdoses involving APAP are. Small in-
218 creases in the dose above what is considered “safe” lead to huge increases
219 in the protein adducts being produced, which in turn can lead to extensive

220 damage to the liver. This threshold behaviour is due entirely to the level
221 of GSH depletion of which leads to the fraction of protein adducts produced
222 increasing 1000-fold over a 3-5g dose (we note that in Remien *et al* the lowest
223 doses for patients receiving treatment is about 5g). The sensitivity of the
224 model solutions to parameter change is explored in the next section, whilst
225 the key parameters governing the threshold dose are established in the analy-
226 sis of Section 4. We note that as $P_S \rightarrow \infty$, the sulphation pathway becomes
227 less significant and it follows that $C_\infty/P_S \rightarrow k_{450}/(k_G + k_{450}) \simeq 0.095$ as
228 $P_S \rightarrow \infty$.

229 Simulations investigating the effect of smaller regular doses are shown in
230 Figure 6, in particular those in the left column represent a typically pre-
231 scribed 1g dose at 4 separate 4 hour intervals over a 5 day period. Here, we
232 observe NAPQI progressively building up in the initial days before settling
233 to a periodic profile. Protein adducts increase linearly, although total levels
234 still remain negligible.

235 The right hand side of Figure 6 plots a higher than recommended chronic
236 dose case, this time with the patient taking 1.5g of APAP every 4 hours. This
237 increase in APAP leads to a rapid depletion of GSH resulting in NAPQI and
238 conjugate levels two orders of magnitude higher than in the 1g case. NAPQI
239 and protein adducts both rise rapidly (after a day) due to the lack of GSH in
240 the system to safely deal with the NAPQI present. The plots once again show
241 dramatic increase in toxic effects (represented by an increase in adducts, C)
242 following a modest overdose.

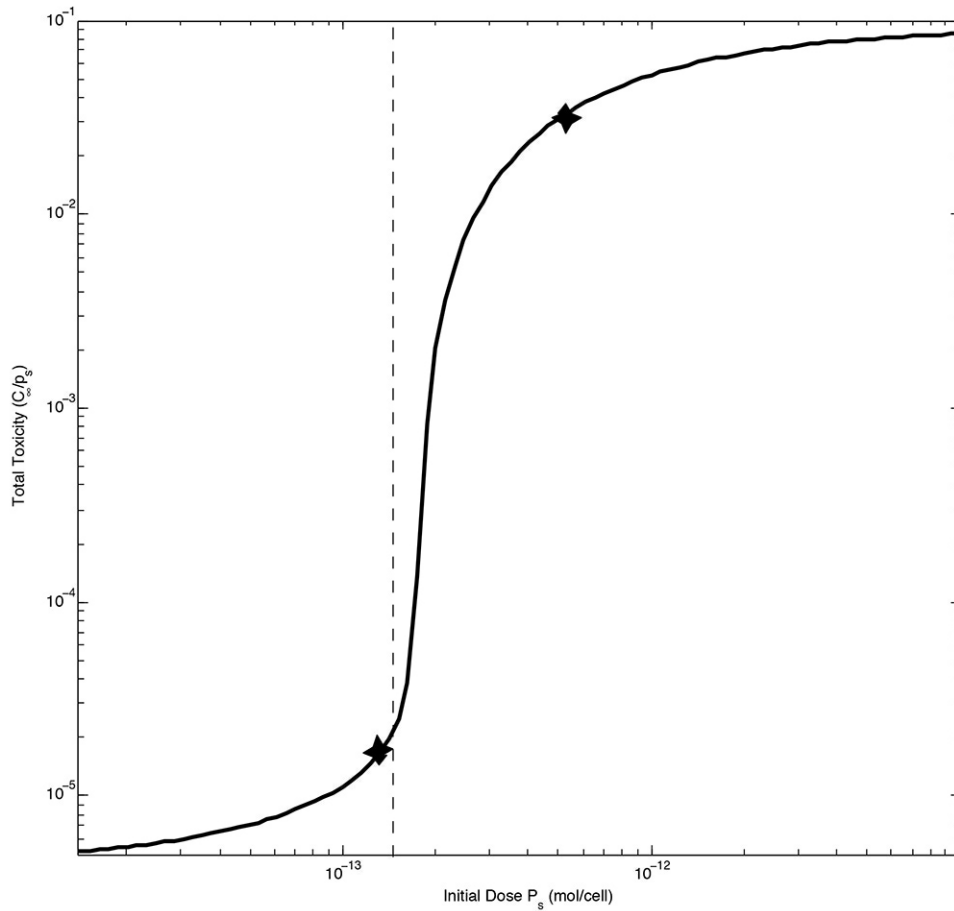


Figure 5: **Plot showing the effect of initial dose (P_0) on final accumulated toxins normalised as the ratio C_∞/P_S .** The dashed line represents the value of P_0^* which is found in section 4.3.1. The stars represent the location of 4g and 16g doses.

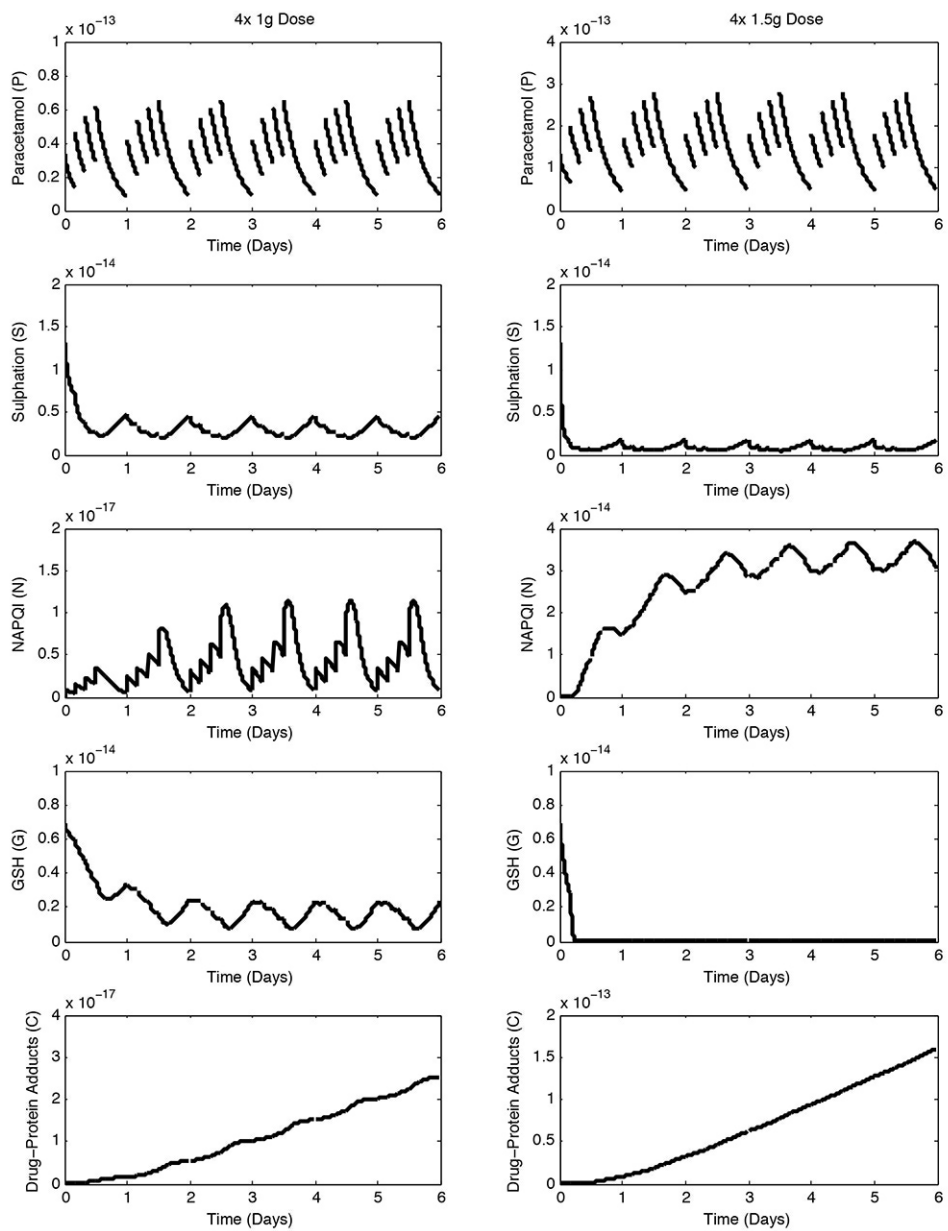


Figure 6: Plots showing evolution of pathways over time in response to a 1g per dose (left) and 1.5g per dose (right) chronic APAP regimen.

243 *3.2. Parameter Sensitivity Analysis*

244 The results in Section 3.1 demonstrated a notable sensitivity to dose.
245 In this section we seek to establish the sensitivity of the model solution to
246 changes in parameter values. To do this systematically we used the Latin
247 Hypercube method implemented using the “lhsdesign” routine in MATLAB.
248 To produce the results that followed, the routine was set up to run 500 iter-
249 ations, which randomly selects parameters between set limits of 3x and $\frac{1}{3}$ x
250 their original value. We used, for the sensitivity test, the total accumulated
251 protein adducts C_∞ (i.e. $C(t)$ as $t \rightarrow \infty$), where we plotted this against each
252 of the model parameters. We look for trends in the resulting graphs, indi-
253 cating higher or lower numbers of protein adducts in response to a change
254 in parameters. To confirm our observation we also examined the Sobol in-
255 dices to estimate the sensitivity of variance of the model output, C , to the
256 variance of the parameters [31]. Defining indices S_i (the first order effect)
257 and S_{T_i} (the total effect index) to be the conditional expectation divided
258 by the unconditional variance and the total output variation due to a given
259 parameter respectively. Then $S_{T_i} - S_i = 0$ indicates that a parameter has no
260 affect on the variance of the model output.

261 Shown in Figure 7 are the results of the sensitivity analysis for the safe
262 dose of 4g. We observe that most of the graphs do not show any sort of trend
263 in response to differing parameter values except that the k_{450} (oxidation rate
264 constant) graph shows an obvious upward trend in protein adducts whilst a
265 downward trend is observed for k_G (glucuronidation rate constant). Here,

266 the Sobol indices are found to be $S_{T_{k_G}} - S_{k_G} \simeq 0.35$, $S_{T_{k_{450}}} - S_{k_{450}} \simeq 0.32$
 267 and $S_{T_{b_G}} - S_{b_G} \simeq 0.2$, while all other values are less than 0.05 confirming
 268 the visual analysis of the parameter sensitivity. Interestingly, the indicated
 269 sensitivity to b_G is not present in the 16g case, suggesting that this is likely
 270 to be an important parameter when doses are near to the “critical level”.
 271 However, as the Sobol Indices for b_G in the overdose case indicate that it has
 272 no significant affect on the model output, we do not feel that any further
 273 analysis is necessary for this parameter. The sensitivity analysis for the
 274 overdose case of 16g is shown in Figure 8. Again we see that changes in
 275 the value of k_{450} and k_G produce the most distinct trends in the model. In
 276 the overdose case, $S_{T_{k_G}} - S_{k_G} \simeq 0.16$ and $S_{T_{k_{450}}} - S_{k_{450}} \simeq 0.06$, while all
 277 other values are again less than 0.05. These are the only 2 parameters with
 278 a notable affect on the model outcome in the overdose regime.

279 This analysis suggests that the key mechanisms that govern paracetamol
 280 metabolism are glucuronidation and oxidation, where increasing k_G reduces
 281 toxicity and increasing k_{450} enhances it. In the parameter range investigated,
 282 PAPS contributes only up to about 10% of APAP metabolism, whereby
 283 sulphation is a secondary process in humans; we note that the sulphation for
 284 rats lies outside the parameter range investigated. Figures 9 and 10 show
 285 the dependence of the total toxins produced, C_∞ , on the two most sensitive
 286 parameters k_{450} and k_G , for the safe and overdose cases. The results were
 287 generated from running the simulation to approximate $C_\infty(t = 50)$, we found
 288 this length of time sufficient to reach a steady state. From Figure 9 we see

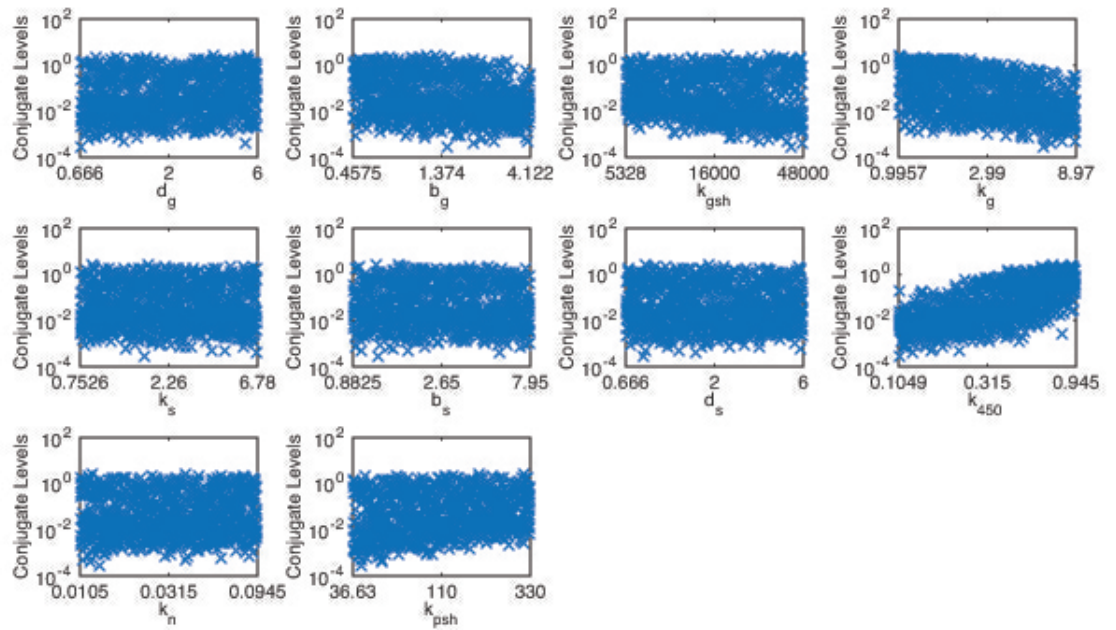


Figure 7: Final accumulated toxic levels from a 4g ('safe') dose against each of the parameters for 1000 iterations of randomly selected values between the limits of $1/3x$ and $3x$ the nominal value listed in Table 2.

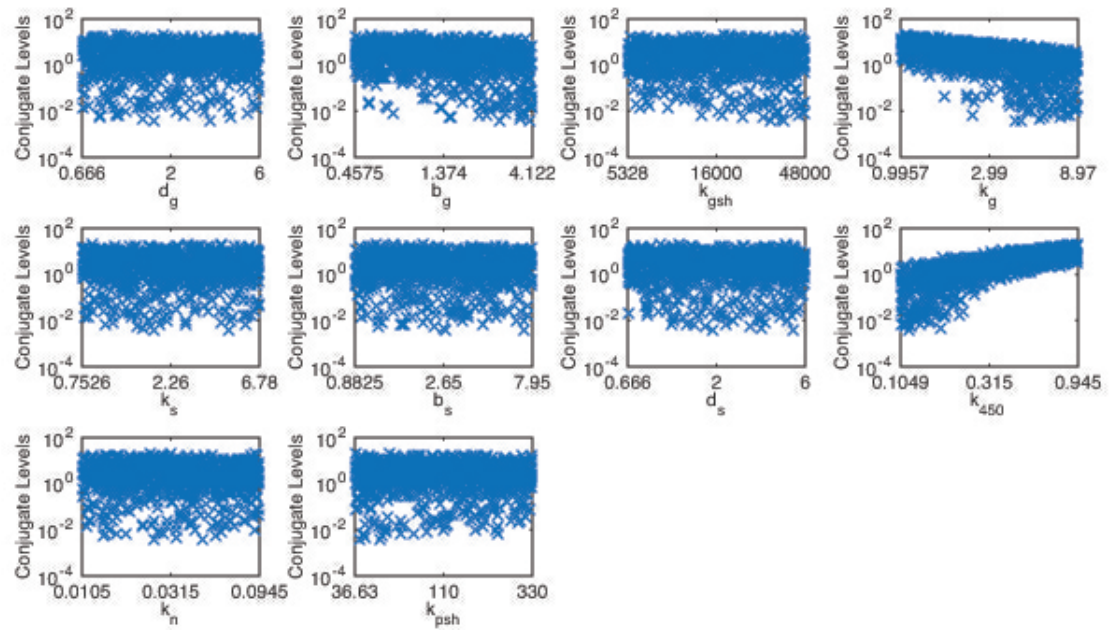


Figure 8: Final accumulated toxic levels from a 16g overdose against each of the paramaters for 1000 iterations of randomly selected values between the limits of $1/3x$ and $3x$ the nominal value listed in Table 2.

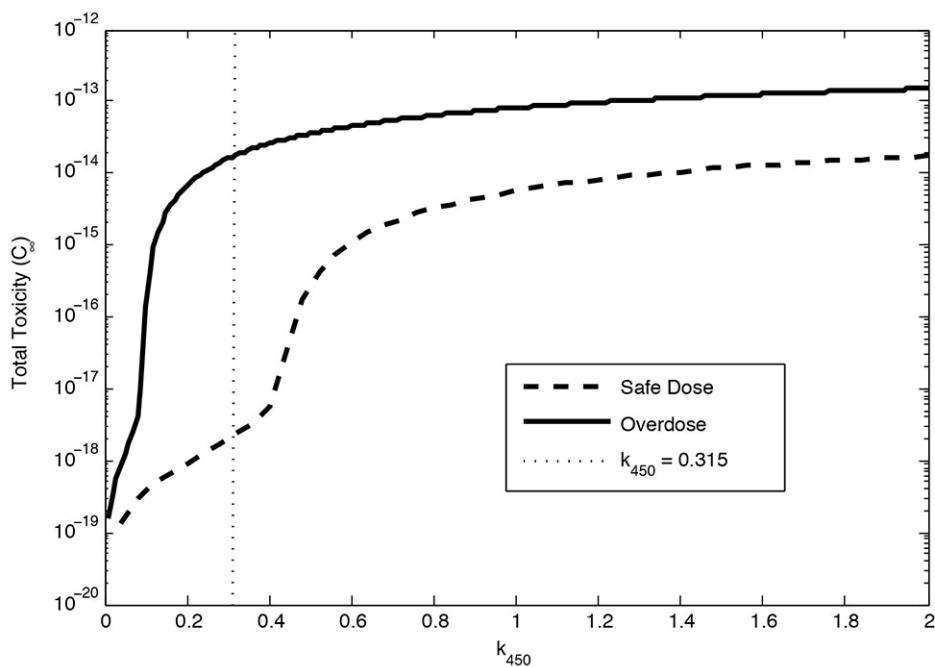


Figure 9: **Total protein adduct formation against k_{450} for the safe (4g, dashed) and overdose (16g, solid) cases.** The dotted line indicates the standard value corresponding to data in Table 2.

289 that increased k_{450} will lead to more APAP being oxidised instead of being
 290 metabolised by sulphation or glucuronidation. This will cause a rise in the
 291 amount of NAPQI in the system, putting more strain on the GSH pathway.
 292 We anticipate that a higher value for k_{450} will lead to more protein adducts
 293 being present in the system and therefore increase the risk of liver damage.

294 The safe dose response shows a steady increase in conjugate levels ini-
 295 tially, followed by a rapid rise in conjugate levels being produced with total
 296 protein adduct formation increasing by over one order of magnitude. A
 297 less dramatic rise in protein conjugates is observed for higher k_{450} values.

298 For our overdose case we see a much faster rise in the total protein adduct
299 formation in response to higher k_{450} levels. We see an increase of approxi-
300 mately three orders of magnitude in response to higher values of k_{450} . After
301 the initial rapid increase in total protein adduct formation, higher values of
302 k_{450} have a much lower affect on C_∞ . Once GSH is depleted in our sys-
303 tem, all NAPQI that is oxidised will produce protein adducts, the rate at
304 which these protein adducts can be formed is then dependent on how quickly
305 NAPQI can be oxidised, this rate is k_{450} . This suggests that after GSH is
306 depleted fully, conjugate production will be proportional to k_{450} . The rate of
307 APAP to NAPQI metabolism can be affected by other factors such as caf-
308 feine consumption [32, 33] and, for example, consumption of anti-convulsant
309 drugs [34] which would result in a higher value of k_{450} .

310 In Figure 10 we observe, as expected, a decline in toxins produced as k_G
311 increases. As with k_{450} , there is a fairly sharp transition between high and
312 low toxicity at a certain value of k_G . We note that a 10-fold increase in k_G is
313 required in the overdose case ($k_G \sim 18$ /day) to produce minimal toxic levels
314 in comparison to the safe doses ($k_G \sim 1.5$ /day). Furthermore, for $k_G \sim 0$
315 /day there is a 10-fold difference in C_∞ levels. This is due simply to more
316 APAP being present for longer in the overdose case. The critical role of GSH
317 exhaustion is highlighted in Figure 11, which plots the numerically predicted
318 minimum value against parameters k_G and k_{450} . Of particular note is how
319 the value of k_G and k_{450} at which the sharp jumps occur correspond to jumps
320 in Figure 9 and 10.

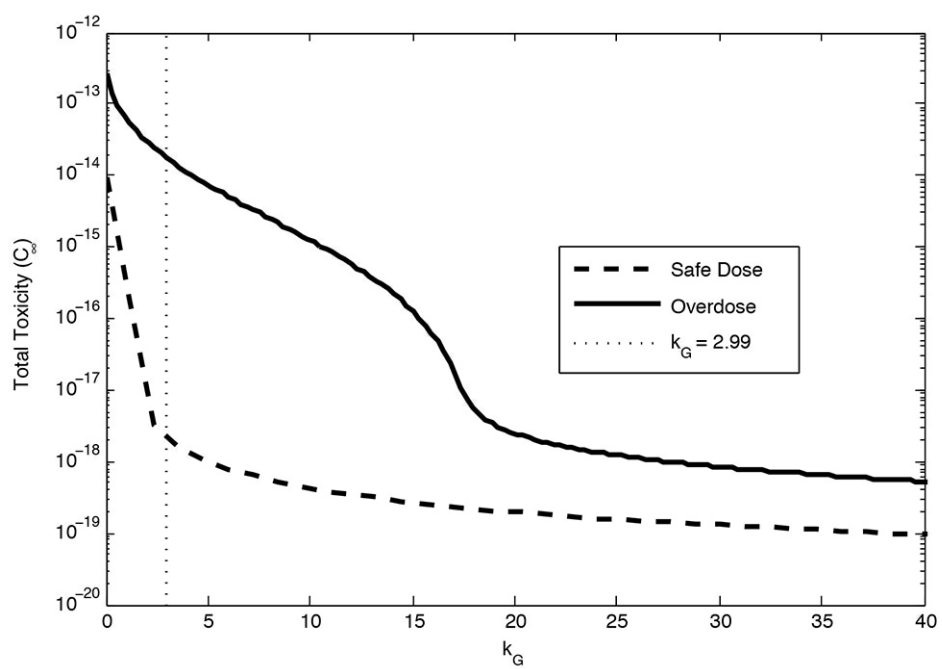


Figure 10: **Total protein adduct formation vs. k_G for the safe (4g, dashed) and overdose (16g, solid) cases.** The dotted line indicates the standard value of k_G found in Table 2.

321 Figure 11 plots the minimum GSH levels in the cell against k_G and k_{450} .
322 As k_G increases we see a rise in the minimum GSH level of 2 orders of
323 magnitude. This suggests that if the glucorination rate drops then GSH
324 could fall low enough to allow protein adducts to form, if for example a person
325 has a genetic or environmental deficiency e.g. co-medication, that reduces the
326 amount of glucorination cofactor it could be dangerous for them to take
327 paracetamol, even in safe doses. We observe in the overdose case that only
328 very large values of k_G have a non-negligible affect on minimum GSH levels.
329 An increase in k_{450} leads to a drop in GSH of over 3 orders of magnitude in the
330 safe dose case, at the normal value of $k_{450} = 0.315$ /day, minimum GSH levels
331 remain high in the cell. However, an increase in k_{450} leads to lower GSH levels
332 which could lead to the formation of protein adducts. Therefore, increased
333 k_{450} can potentially lead to liver damage via protein adduct formation even
334 in safe dose cases.

335 3.3. Cellular dose variation

336 The structure of the liver lobule means that cells closer to the portal vein
337 are likely to receive more of the drug. As a consequence, there will be a dis-
338 tribution of drug dosage between cells in the liver. Some cells which receive
339 higher doses are more likely to be damaged than others. Furthermore, dif-
340 ferences in micro-environment due to proximity to blood vessels and oxygen
341 gradients could also affect drug metabolism. The effects of the the micro-
342 environment will be subject to a future publication, and here we investigate

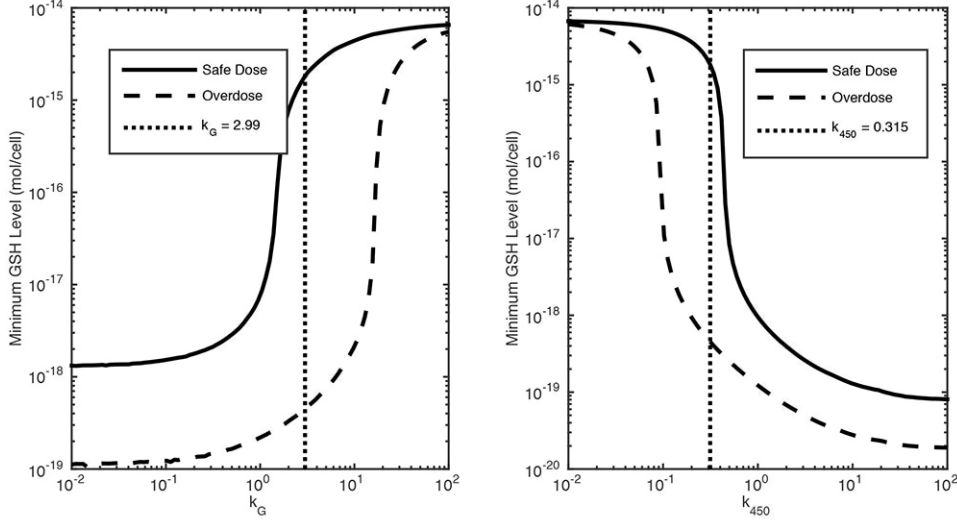


Figure 11: **Plot showing minimum GSH levels in the hepatocytes against k_G (left) and k_{450} (right).** The dotted vertical lines indicate the original parameters values from Table 2.

343 how the spread of drug dosing effects the probability of cell death given a
 344 dose.

345 In Figure 12, we assume that a dose of paracetamol is log-normally dis-
 346 tributed between the hepatocytes in the liver. We assumed that a lethal dose
 347 for cells (p_L) is 5 times the daily safe dose [22] and we plotted the probability
 348 $p > p_L$, given a mean dose $\log(\bar{p}_s)$ and variance σ^2 , against mean dose. We
 349 observe that higher standard deviations lead to a less sharp profile. It is
 350 expected that 70% total cell death will lead to the death of the patient [22],
 351 in our simulations we see that this occurs from $\sim 7 \times 10^{-13}$ mol/cell (ap-
 352 prox. 5 times the standard dose) to $\sim 9 \times 10^{-13}$ mol/cell (approx. 7 times
 353 the standard dose). Interestingly, we also see that greater variation between

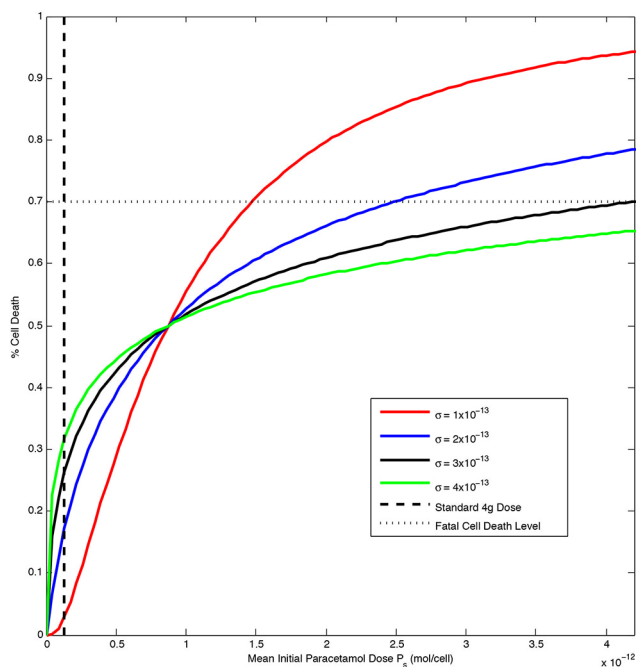


Figure 12: Plot showing the fraction of cell death in response to an increasing initial paracetamol dose, normally distributed amongst cells.

354 hepatocytes leads to more deaths at lower doses, but less death at higher
 355 doses. This suggests that variation is a positive property for the popula-
 356 tion on average, for survival against a very large, single dose. However, this
 357 doesn't necessarily mean it is a positive property for the individual.

358 4. Timescale Analysis

359 In the previous section we were able to get some insight into how certain
 360 parameters effect the predicted toxicological outcome. In this section we will
 361 employ singular perturbation theory to get a much better analytical under-
 362 standing of APAP metabolism according to the model. Close examination

363 of Figure 4 reveals the existence of distinct timescales, starting with a rapid
 364 decline in PAPS and GSH followed by longer timescales for recovery. To ap-
 365 ply this theory we first non-dimensionalise the system of equations (1) - (5).
 366 Using the data values in Table 2, we express the new parameters in terms
 367 of a single small parameter ϵ (i.e. $\epsilon \ll 1$), which will be exploited in the
 368 analysis. We will summarise the main results here, and we refer the reader
 369 to the supplemental material for full details.

370 4.1. Non-dimensionalisation

To aid the analysis we rescale our variables in order to eliminate units, which allows comparison of variables and parameters in terms of their magnitude, so that the dominant and negligible mechanisms can be systematically identified. Since glucuronidation is the dominant metabolism route for APAP, we rescale time with parameter k_G ; using the value in Table 2, the dimensionless time $\hat{t} = 1$ thus represents about 8 hours. We rescale PAPS and GSH with their untreated levels and rescale APAP, NAPQI and protein adducts to a reference value P_0 which represents the liver cell level of a 4g dose i.e. $P_0 = 1.32 \times 10^{-13}$ mol/cell. The rescalings are thus,

$$t = \frac{1}{k_G} \hat{t}, \quad P = P_0 \hat{p}, \quad S = \frac{b_S}{d_S} \hat{s}, \quad N = P_0 \hat{n}, \quad G = \frac{b_G}{d_G} \hat{g}, \quad C = P_0 \hat{c}.$$

and we note the standard dose concentration P_0 corresponds to $\hat{p} = 1$. The

dimensionless system of equations is then

$$\frac{d\hat{p}}{d\hat{t}} = -\hat{\alpha}_S^* \hat{s} \hat{p} - \hat{p} - \epsilon \hat{p} + \epsilon^2 \hat{k}_N^* \hat{n}, \quad (7)$$

$$\frac{d\hat{s}}{d\hat{t}} = -\frac{\hat{\alpha}_S^* \hat{\phi}_S^* \hat{s} \hat{p}}{\epsilon} + \hat{\delta}_S^* (1 - \hat{s}), \quad (8)$$

$$\frac{d\hat{n}}{d\hat{t}} = \epsilon \hat{p} - \epsilon^2 \hat{k}_N^* \hat{n} - \frac{\hat{k}_{PSH}^*}{\epsilon} \hat{n} - \frac{\hat{\alpha}_G^*}{\epsilon^3} \hat{n} \hat{g}, \quad (9)$$

$$\frac{d\hat{g}}{d\hat{t}} = -\frac{\hat{\alpha}_G^* \hat{\phi}_G^*}{\epsilon^4} \hat{n} \hat{g} + \hat{\delta}_G^* (1 - \hat{g}), \quad (10)$$

$$\frac{d\hat{c}}{d\hat{t}} = \frac{\hat{k}_{PSH}^*}{\epsilon} \hat{n}, \quad (11)$$

where the rescaled parameters are listed in Table 3. The third column of Table 3 lists the value of the parameter, and for the purpose of the analysis we will rewrite them in terms of the small parameter $\epsilon = k_{450}/k_G \simeq 0.1$ guided by magnitudes indicated in the 4th column; thus starred values in equations (7)-(11) are defined as $\hat{k}_N = \epsilon^2 \hat{k}_N^*$, $\hat{\alpha}_S = \hat{\alpha}_S^*$ etc. These dimensionless variables are subject to the initial conditions

$$\hat{p}(0) = P_S, \quad \hat{s}(0) = 1, \quad \hat{n}(0) = 0, \quad \hat{g}(0) = 1, \quad \hat{c}(0) = 0,$$

371 recalling that $P_S = 1$ represents the 4g dose case. Henceforth, we will drop
 372 the hats and the *'s for clarity. In Section 4.2 we provide an overview of
 373 the main mathematical results and we then give biological interpretations in
 374 Section 4.3

375 *4.2. Application of singular perturbation theory*

376 The system (7)-(11) will be analysed in the limit $\epsilon \rightarrow 0$. Using singular
 377 perturbation theory we can perform this analysis systematically and formally
 378 reduce the full system to a sequence of timescales in which the system reduces
 379 to a simpler solvable one in each timescale. This will enable us to identify
 380 when a particular process is important and determine an approximation to
 381 key quantities such as critical dose in terms of the model parameters. Full
 382 details of the analysis is given in the supplementary material and we present
 383 only the “highlights” below. A summary of this analysis and the important
 384 timescales and events is provided in Section 4.3. We note that toxic levels of
 385 protein adducts will be $c = O(\epsilon^2)$ as shown in Figure 5.

Table 3: Table of dimensionless parameters, their values and the assumed value relative to the reference small parameter ϵ .

Parameter	Definition	Value	Order in terms of ϵ
\hat{k}_{450}	k_{450}/k_G	0.105	ϵ
\hat{k}_N	k_N/k_G	0.0105	$\mathcal{O}(\epsilon^2)$
$\hat{\alpha}_S$	$k_S b_S / d_S k_G$	1	$\mathcal{O}(1)$
$\hat{\phi}_S$	$P_0 d_S / b_S$	10	$\mathcal{O}(\frac{1}{\epsilon})$
$\hat{\delta}_S$	d_S / k_G	0.668	$\mathcal{O}(1)$
\hat{k}_{PSH}	k_{PSH} / k_G	36.8	$\mathcal{O}(\frac{1}{\epsilon})$
$\hat{\alpha}_G$	$k_{GSH} b_G / d_G k_G$	3680	$\mathcal{O}(\frac{1}{\epsilon^3})$
$\hat{\phi}_G$	$P_0 d_G / b_G$	19.3	$\mathcal{O}(\frac{1}{\epsilon})$
$\hat{\delta}_G$	d_G / k_G	0.668	$\mathcal{O}(1)$

386 4.2.1. $t = O(\epsilon^3)$

On introduction of the APAP bolus there is a rapid adjustment over $t = O(\epsilon^3)$, the first 30 seconds or so, in which NAPQI is produced at very low levels. Denoting variables in this timescale with a superscript $*$, we write

$$t = \epsilon^3 \tau^*, \quad p = p^*, \quad s = s^*, \quad n = \epsilon^4 n^*, \quad g = g^*, \quad c = \epsilon^6 c^*.$$

These rescalings are then substituted into our dimensionless equations (7)-(11), subject to $p^* = P_S, s^* = 1, g^* = 1, n^* = 0$ and $c^* = 0$ at $t^* = 0$. In each timescale we seek solutions of the form

$$p(\tau^*) = p_0^*(\tau^*) + \epsilon p_1^*(\tau^*) + \epsilon^2 p_2^*(\tau^*) + \dots$$

and likewise for the other variables. Substituting these expansions into our equations we obtain to leading order $p^* \sim P_S, s^* \sim 1$ and $g^* \sim 1$ (correction terms can be found in our supplementary material) and

$$n^* \sim \frac{P_S}{\alpha_G} (1 - e^{-\alpha_G \tau^*}),$$

$$c^* \sim \frac{k_{PSH} P_S (\alpha_G \tau^* + e^{-\alpha_G \tau^*} - 1)}{\alpha_G^2}.$$

387 In this short initial timescale, APAP, PAPS and GSH remain relatively
 388 unchanged and NAPQI equilibrates to a negligible $O(\epsilon^4)$ level. As $t^* \rightarrow \infty$,
 389 NAPQI settles to $n \sim \epsilon^4 (P_S / \alpha_G)$ and $c \sim \epsilon^6 (k_{PSH} P_S \tau^* / \alpha_G)$. We note here
 390 that as $\tau^* \rightarrow \infty, n \sim \epsilon^4 P_S / \alpha_G$, this represents the amount of NAPQI formed

391 if PAPS and GSH remain at their pretreatment levels. There is no change
 392 at leading order of p, s and g , however the correction terms become $O(1)$ at
 393 $\tau^* = O(\epsilon^{-2})$ i.e. at $t = O(\epsilon)$.

394 *4.2.2. $t = O(\epsilon)$*

It is on this timescale at which sulphation is most prominent. We introduce $t = \epsilon\bar{\tau}$ and the relevant rescalings are

$$p = \bar{p}, \quad s = \bar{s}, \quad n = \epsilon^4 \bar{n}, \quad g = \bar{g}, \quad c = \epsilon^4 \bar{c}.$$

Substituting the expansions above, $\bar{p} \sim \bar{p}_0 + \epsilon\bar{p}_1$ etc. into (7)-(11) and solving leads to

$$\begin{aligned} \bar{p} &\sim P_S + \epsilon \left(\frac{1}{\phi_S} (e^{-\alpha_S \phi_S P_S \bar{\tau}} - 1) - P_S \bar{\tau} \right), \\ \bar{s} &\sim e^{-\alpha_S \phi_S P_S \bar{\tau}}, \\ \bar{g} &\sim 1 + \epsilon(-\phi_G P_S \bar{\tau}), \\ \bar{n} &\sim \frac{P_S}{\alpha_G}, \\ \bar{c} &\sim \frac{k_{PSH} P_S}{\alpha_G} \bar{\tau}. \end{aligned}$$

395 In this timescale, we see that sulphate levels drop rapidly whilst APAP is rela-
 396 tively steady. Biologically this is due to the conjugation of APAP and PAPS,
 397 leading to declining PAPS levels in the cell. The parameters used suggest
 398 that the pretreated PAPS concentration is $O(\epsilon P_S)$ so, at best, sulphates are

399 only able to metabolise an $O(\epsilon)$ fraction of the drug. There is also an increase
 400 in protein adducts, although they are still only present in very low amounts.
 401 We note as $\bar{\tau} \rightarrow \infty$, $\bar{p} \sim P_S - \epsilon(\phi_S^{-1} + P_S \bar{\tau})$, where ϵ/ϕ_S represents the
 402 amount of APAP being metabolised by the sulphation pathway. There is a
 403 transition timescale $t = \epsilon \eta_1(\epsilon) + O(\epsilon)$, where $\eta_1 = \ln(1/\epsilon)/\alpha_S \phi_S P_S$, in which
 404 sulphate reaches a minimum constant level, namely $s \sim \epsilon \delta_S / \alpha_S \phi_S P_S$; sul-
 405 phation makes no further contribution to APAP metabolism at leading order.
 406 The expansion breaks down when $\bar{\tau} = O(1/\epsilon)$, corresponding to $t = O(1)$,
 407 when APAP concentration starts to significantly drop.

408

409 4.2.3. $t = O(1)$

In this timescale, we have two separate divergent cases. One in which
 we have sufficient amounts of GSH in the system to conjugate NAPQI, the
 other is characterised by a rapid drop in GSH and potential toxin build up.
 The critical dose at which the two cases diverge is

$$P_S^* = \frac{\delta_G^{\frac{\delta_G}{\delta_G - 1}}}{\phi_G}, \quad (12)$$

410 such that, $P_S < P_S^*$ can be classified as “safe” and $P_S > P_S^*$ can be considered
 411 a potential overdose. We note here that we have assumed that $\delta_G \neq 1$, we will
 412 omit details for the coincidental case of $\delta_G = 1$ (i.e. $\delta_G = k_G$ in dimensional
 413 terms).

In both cases, we adopt the following rescaling.

$$t = \tilde{\tau}, \quad p = \tilde{p}, \quad s = \epsilon \tilde{s}, \quad n = \epsilon^4 \tilde{n}, \quad g = \tilde{g}, \quad c = \epsilon^3 \tilde{c}.$$

Expanding these variables in the usual way, and solving the resulting system yields

$$\tilde{p} \sim P_S e^{-\tilde{\tau}} - \epsilon \left(e^{-\tilde{\tau}} \left(\frac{\delta_S}{\phi_S} - P_S \tilde{\tau} \right) - \frac{\delta_S}{\phi_S} \right), \quad (13)$$

$$\tilde{s} \sim \frac{\delta_S e^{\tilde{\tau}}}{\alpha_S \phi_S P_S}, \quad (14)$$

$$\tilde{n} \sim \frac{P_S e^{-\tilde{\tau}}}{\alpha_G \left(\frac{\phi_G P_S}{\delta_G - 1} (e^{-\delta_G \tilde{\tau}} - e^{-\tilde{\tau}}) + 1 \right)} = \frac{P_S e^{-\tilde{\tau}}}{\alpha_G \Psi(\tilde{\tau})}, \quad (15)$$

$$\tilde{g} \sim \frac{\phi_G P_S}{\delta_G - 1} (e^{-\delta_G \tilde{\tau}} - e^{-\tilde{\tau}}) + 1 = \Psi(\tilde{\tau}), \quad (16)$$

$$\tilde{c} \sim k_{PSH} \int_0^{\tilde{\tau}} \tilde{n}(\tilde{\tau}) d\tilde{\tau}. \quad (17)$$

414 Here, APAP is metabolised such that $p \sim P_S e^{-\tau}$ (due to glucuronidation
 415 at leading order) and that PAPS is recovering, noting that $s = O(\epsilon)$ and
 416 therefore is not contributing to APAP metabolism at leading order. We also
 417 note that \tilde{c} is unsolvable in this timescale, but we can deduce behaviour as
 418 $\tilde{\tau} \rightarrow \tilde{\tau}^*$ (see below), as explained in the supplementary material.

The divergence depends on the function

$$\Psi(\tilde{\tau}) = 1 + \frac{\phi_G P_S}{\delta_G - 1} (e^{-\delta_G \tilde{\tau}} - e^{-\tilde{\tau}}), \quad \forall \tilde{\tau} > 0$$

419 whereby if $\Psi(\tilde{\tau}) > 0$, $\forall \tilde{\tau} > 0$, then \tilde{n} and \tilde{g} remain positive and $O(1)$, this
420 is our safe dose case. If at $\tilde{\tau} = \tilde{\tau}^*$, such that $\Psi(\tilde{\tau}^*) = 0$, then $\tilde{n} \rightarrow \infty$ in
421 finite time $\tilde{\tau} \rightarrow \tilde{\tau}^*$ whilst $\tilde{g} \rightarrow 0$. The divergence condition ($P_S = P_S^*$) is
422 determined by assuming that $\Psi(\tilde{\tau}^*) = 0$ is a turning point at $\tilde{\tau} = \tilde{\tau}^*$, i.e.
423 solving $\Psi(\tilde{\tau}^*) = 0$ and $\Psi'(\tilde{\tau}^*) = 0$ simultaneously leading to $t^* = \ln \delta / (\delta - 1)$.
424 We note that the safe and overdose cases can be connected smoothly by
425 analysis in the region of $P_S = P_S^* + \epsilon\theta$, where $\theta \simeq O(1)$. The results are
426 omitted as they are not of biological significance other than it reveals that
427 the jump region observed in Figure 5 is of $O(\epsilon) = O(k_{450}/k_G)$ in size.

428 In the overdose case, when $P_S > P_S^*$, breakdown occurs when $t \sim \mu_1(\epsilon)$,
429 where $\mu_1(\epsilon)$ is defined such that $\Psi(\mu_1(0)) = 0$; and $\tilde{g} = O(\epsilon)$ and $\tilde{n} = O(1/\epsilon)$.
430 Here, $\mu_1(\epsilon)$ is the time at which hepatocytes no longer have an effective
431 means of dealing with NAPQI. It is straightforward to show that $\mu_1(\epsilon)$ is a
432 decreasing function of P_S and d_g , i.e. more drug and less glutathione reduces
433 the time interval, as expected. We further note that given $\Psi(\mu_1) = 0$ and
434 $\Psi'(\mu_1) < 0$ we can show that $\phi_G P_S e^{-\mu_1} > \delta_G$; this result is utilised in Section
435 4.2.5. In the overdose case, breakdown occurs when $t \sim \tilde{\tau}^* = \mu_1(\epsilon)$, where
436 $\Psi(\mu_1(0)) = 0$ and $\Psi(\tilde{\tau}) = O(\epsilon)$, so that $\tilde{g} = O(\epsilon)$ and $\tilde{n} = O(1/\epsilon)$, this is
437 discussed in Section 4.2.5.

438 4.2.4. Safe dose case ($P_S < P_S^*$)

Here, the drug decays exponentially (predominantly by glucuronidation)
and $\tilde{g} = O(1)$ throughout, i.e. GSH is able to handle the NAPQI being

produced. Meanwhile sulphate cofactors are recovering but only at very low levels. Protein adducts attain their maximum level i.e. $O(\epsilon^3)$, namely

$$c_\infty \sim \epsilon^3 \frac{k_{PSH} P_S}{\alpha_G} \int_0^\infty \frac{e^{-\tau}}{\Psi(\tau)} d\tau$$

439 There is a further timescale at $t = \ln(1/\epsilon) + O(1)$ in which the sulphation
440 factors, now $O(1)$, continue to recover, and return to pre-treatment state.

441 *4.2.5. $t = \mu_1(\epsilon) + O(1)$ (overdose).*

GSH and NAPQI continue to drop and rise, respectively, over a series of intermediate timescales until the current one describing the time period at which GSH is at its minimum level. We rescale our variables as follows

$$t = \mu_1 + \check{\tau}, \quad p = \check{p}, \quad s = \epsilon \check{s}, \quad n = \epsilon^2 \check{n}, \quad g = \epsilon^2 \check{g}, \quad c = \epsilon \check{c}.$$

We then expand our variables as before, substitute them into (7) - (11) and solve to find

$$\begin{aligned} \check{p} &\sim P_S e^{(-\mu_1 - \check{\tau})}, \\ \check{s} &\sim \frac{\delta_S e^{\mu_1}}{\alpha_S \phi_S P_S}, \\ \check{n} &\sim \frac{\phi_G P_S e^{-\mu_1 - \check{\tau}} - \delta_G}{k_{PSH} \phi_G}, \\ \check{g} &\sim \frac{\delta_G k_{PSH}}{\alpha_G (\phi_G P_S e^{-\mu_1 - \check{\tau}} - \delta_G)}, \\ \check{c} &\sim P_S e^{-\mu_1} (1 - e^{-\check{\tau}}) - \frac{\delta_G}{\phi_G} \check{\tau} \end{aligned}$$

442 In this timescale APAP levels continue to drop while sulphates remain steady.
 443 Protein adducts approach their maximum level while NAPQI production be-
 444 gins to slow and GSH levels begin to rise as APAP levels decline. The solu-
 445 tions in this timescale breakdown as $\tilde{\tau} \rightarrow \mu_2(\epsilon)^-$, with $\mu_2(0) = \ln(\phi_G P_S / \delta_G) -$
 446 $\mu_1(0)$, where $\check{g} = O(1/\epsilon)$ and $\check{n} = O(\epsilon)$. After this timescale, NAPQI levels
 447 begin to decline. As $\tilde{\tau} \rightarrow \mu_2^-$, c attains its maximum value to leading order,
 448 i.e. $c_\infty \sim \epsilon(P_S e^{-\mu_1}(1 - e^{-\mu_2}) - \mu_2 \delta_G / \phi_G)$. We can show that the amount
 449 of protein adducts increases with P_S (i.e. higher initial dose) and ϕ_G (less
 450 GSH present) as would be expected.

451 *4.2.6. $t = \mu_1(\epsilon) + \mu_2(\epsilon) + O(1)$ (overdose).*

This timescale follows a series of intermediate timescales in which GSH rapidly recovers and NAPQI diminishes. Here, the rescalings are

$$t = \mu_1 + \mu_2 + \tau^\circ, \quad p = p^\circ, \quad s = \epsilon s^\circ, \quad n = \epsilon^4 n^\circ, \quad g = g^\circ, \quad c = \epsilon c^\circ$$

and proceeding as before

$$\begin{aligned}
p^\circ &\sim P_S e^{-\mu_1 - \mu_2 - \tau^\circ} \\
s^\circ &\sim \frac{\delta_S e^{\mu_1 + \mu_2 + \tau^\circ}}{\alpha_S \phi_S P_S} \\
n^\circ &\sim \frac{P_S e^{-\mu_1 - \mu_2 - \tau^\circ}}{\alpha_G \left(\frac{\phi_G P_S e^{-\mu_1 - \mu_2}}{\delta_G - 1} (e^{-\delta_G \tau^\circ} - e^{-\tau^\circ}) + 1 \right)} \\
g^\circ &\sim \frac{\phi_G P_S e^{-\mu_1 - \mu_2}}{\delta_G - 1} (e^{-\delta_G \tau^\circ} - e^{-\tau^\circ}) + 1 \\
c^\circ &\sim P_S e^{-\mu_1} (1 - e^{-\mu_2}) - \frac{\delta_G}{k_G} \mu_2
\end{aligned}$$

452 Here we see that APAP levels continue to drop exponentially, allowing PAPS
453 levels to rise exponentially. GSH levels are now $O(1)$ and will soon recover to
454 its pretreated level, whilst the tiny amounts of NAPQI that remain rapidly
455 decrease. We now have GSH returning to pretreated levels as NAPQI dimin-
456 ishes.

457 After this, the only timescale of significance is $\tau^\circ = \ln(1/\epsilon) + O(1)$,
458 whereby $p \rightarrow O(\epsilon)$ and $s \rightarrow O(1)$, i.e. their pretreated levels.

459 4.2.7. Comparison with numerics

460 Figure 13 shows the evolution of the dimensionless APAP, PAPS and
461 GSH concentrations against dimensionless time in an overdose case (left).
462 As expected, the agreement improves as ϵ decreases (right).

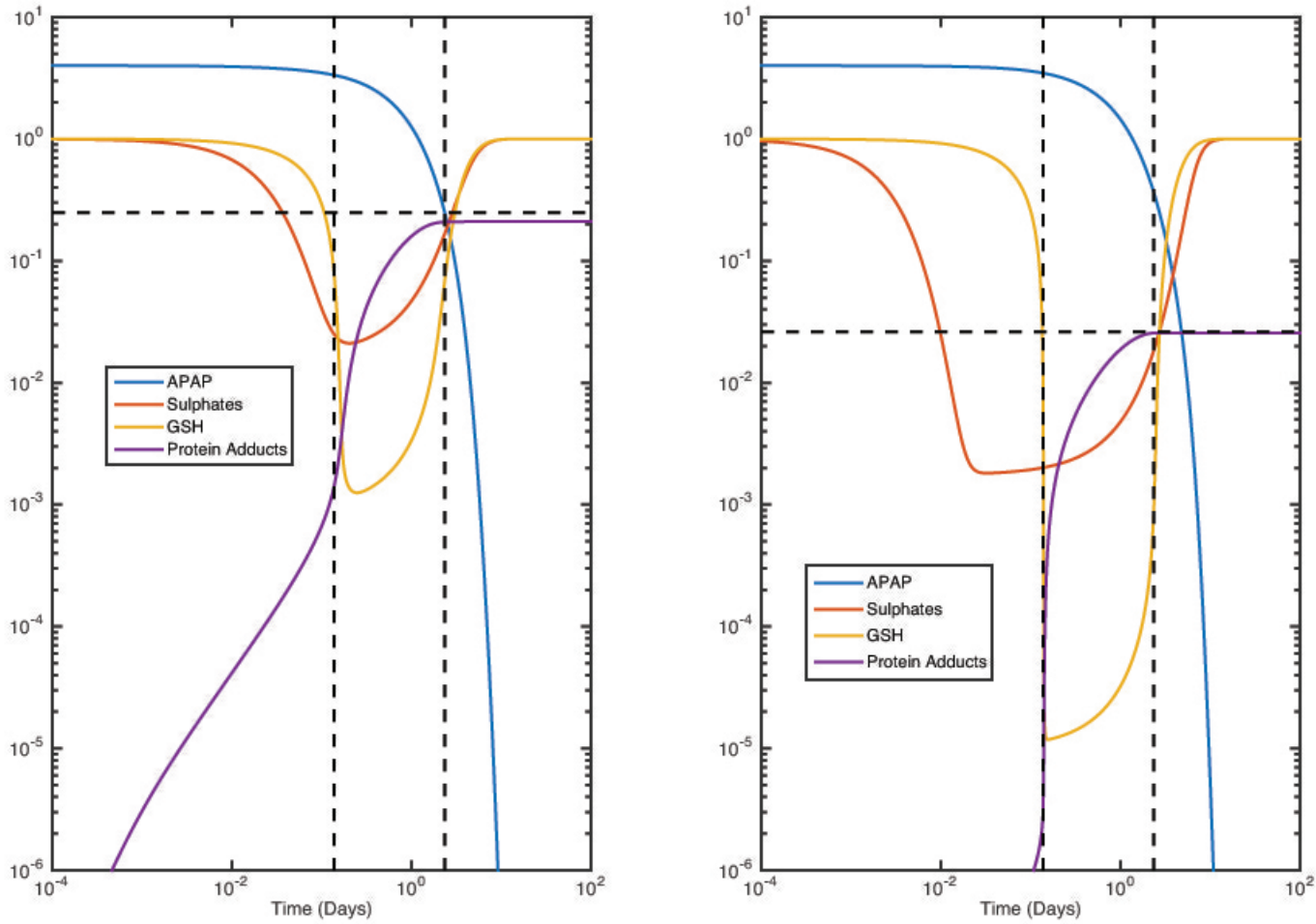


Figure 13: Plots of APAP, Sulphates, Drug-Protein Adducts and GSH against dimensionless time in an overdose case, the left hand graph when $\epsilon = 0.105$ and the right hand graph when $\epsilon = 0.105^2$. The horizontal dashed line shows our analytical estimate for C_∞ , the vertical dashed lines show the estimates for GSH collapse and recovery as discussed in section 4.3.4, 2.3.5 and 2.3.6.

463 *4.3. Timescale Analysis Summary*

464 Here we summarise the important events and timescales from the previ-
465 ous section, expressing the key dimensionless quantities in their dimensional
466 form.

467 *4.3.1. Critical paracetamol concentration*

In section 4.2.3, where $t = O(1)$ we observe a divergence between our safe
and overdose cases. This divergence occurs at a critical concentration

$$P_S^* \sim \left(\frac{d_G}{k_G} \right)^{k_G/(d_G - k_G)} \frac{b_G}{k_G}, \quad (18)$$

468 where $P_S^* = 1.47 \times 10^{-13}$ mol/cell using the data available in Table 2. We note
469 4g translates to a concentration of 1.32×10^{-13} mol/cell and our divergence
470 happens at a point 11% above this dose. This highlights the relatively low
471 tolerance the liver has in response to large bolus doses of paracetamol.

472 *4.3.2. Exhaustion of sulphate*

Our analysis shows that sulphate is exhausted in the intermediate timescale
between 4.2.2 and 4.2.3. The approximate timescale for exhaustion of sul-
phate is

$$t \sim \frac{k_{450}}{k_G k_S P_S} \ln(k_G/k_{450}),$$

473 which using the data is $t \sim 12$ minutes for a 4g dose. After this point the
474 pathway saturates and we a greater proportion of APAP being metabolised
475 into NAPQI, impacting GSH levels. We note that the estimate is only log-

476 arithmically accurate and will not be as precise as those in Section 4.3.1,
 477 4.3.4 and 4.3.5 are; nevertheless it makes explicit how much faster PAPS is
 478 exhausted in response to an increased drug dose.

479 *4.3.3. Sulphate recovery*

In both safe and overdose cases, we see sulphate recover at $t = \ln(1/\epsilon)$,
 in dimensional parameters this is

$$t \sim \frac{1}{k_G} \ln \left(\frac{k_S P_S k_G}{d_S k_{450}} \right).$$

480 Using the data this equates to about 40 hours after ingestion for a 4g dose;
 481 though we note, like that of Section 4.3.2, this estimate is only logarithmically
 482 accurate. Sulphate recovery is a long term process and the liver takes a long
 483 time to recover from a high paracetamol dose. In the case where a person
 484 uses paracetamol chronically to deal with pain then this long recovery time
 485 could impact how well the liver can deal with multiple doses. We note, as
 486 expected, that the recovery time is extended with dose, but in a sublinear
 487 fashion.

488 *4.3.4. GSH depletion*

In our overdose case, when $P_S > P_S^*$ we observe a collapse in GSH levels
 at $t \sim \mu_1$ (Section 4.2.3). Where μ_1 satisfies the implicit equation

$$1 + \frac{k_G d_G P_S}{b_G (d_G - k_G)} (e^{-d_G \mu_1} - e^{-k_G \mu_1}) = 0.$$

489 This equation cannot be solved directly to find μ_1 but given values of the
 490 parameters, the equation can be solved using the Newton-Raphson method.
 491 Using the data in Table 2 gives $\mu_1 \approx 0.046$ for the overdose case, which using
 492 dimensionless parameters is $\mu_1 \approx 0.138$ which is in good agreement with
 493 the numeric values shown in Figure 13. We then show that mathematically
 494 we can improve our estimate by reducing the size of ϵ . Similarly, we find
 495 $t \sim \mu_2 \approx 2.358$ in the overdose case, again providing good agreement with
 496 the numeric values shown in Figure 13. In terms of dimensional parameters
 497 this gives us $\mu_2 \approx 0.79$, which is discussed further in section 4.3.5.

498 4.3.5. GSH Recovery

Again looking at the case where $P_S > P_S^*$, the time for GSH recovery is
 given by

$$t \sim \frac{1}{k_G} \ln \left(\frac{k_G P_S}{b_G} \right).$$

499 Which is approximately 8.9 hours for a 4g dose and 20 hours for a 16g dose.
 500 People regularly taking high doses of APAP can cause damage by not allowing
 501 time for GSH recovery and subsequently protein adduct formation could be
 502 high. Again, the plot in Figure 13 shows how this estimate of GSH recovery is
 503 accurate for our model and how smaller values of ϵ (i.e. a decreasing k_{450}/k_G
 504 ratio) increase the accuracy of our estimate.

505 *4.3.6. Total protein conjugate formation, C_∞*

The total concentration of drug-protein adducts in in the overdose case, $P_S > P_S^*$, is

$$C_\infty \sim \frac{k_{450}P_S e^{-k_g\mu_1}}{k_G} - \frac{b_G k_{450}}{k_G^2} (1 + k_G\mu_2)$$

506 We note that the accumulated drug-protein adducts total is unaffected (to
507 leading order) by parameters associated with PAPS. Moreover, we can show
508 that C_∞ increases with an increasing initial APAP dose and CYP reaction
509 rate, and decreases in response to an increasing GSH production rate and
510 glucuronidation reaction, as expected. Figure 13 shows that this offers a
511 fair prediction of maximum drug-protein adduct levels. We note that no pa-
512 rameters associated with sulphation have an affect on the final accumulation
513 of protein conjugate formation and suggest that the sulphation pathway is
514 unlikely to be a suitable target for an effective new treatment against the tox-
515 icological effects of an APAP overdose. However, we should note that even
516 though sulphates are “exhausted” by time $t \sim \ln(k_G/k_{450})/k_G P_S$ it is still
517 removing APAP at around the same rate as the oxidative pathway between
518 timescales 4-10 (see supplemental material).

519 **5. Discussion**

520 In this paper, we have derived a cell scale mathematical model which
521 describes the metabolism of APAP in hepatocytes. In order to obtain insights
522 into this system using analytical methods, we simplified the full metabolic

523 pathway to one that still maintains the three major pathways.

524 The simulations demonstrated that the model captures the expected dy-
525 namics of metabolism and, in particular, the distinguishing dynamics be-
526 tween the safe and overdose cases. We observe the expected drops in both
527 sulphate and GSH levels in the safe dose case and our overdose simulations
528 have both pathways dropping rapidly to very low levels, which is what we
529 expect from clinical observation. The results show that a 4x dose of APAP
530 can lead to a 100-10000x increase in the amount of protein adducts being
531 formed.

532 Our sensitivity analysis has enabled us to identify the most sensitive pa-
533 rameters in our model, we can use these to guide the research of biologists
534 which will then provide further insight and help us to refine our model. The
535 analysis in Section 3.2 showed that the key parameters are k_G (the rate con-
536 stant for glucuronidation) and k_{450} (the rate of oxidation); the other parame-
537 ters have secondary effects on the dynamics and, in particular, the sulphation
538 pathway is less influential than glucuronidation and oxidation. There is on-
539 going work by the authors examining adaptive responses to chronic dosing.
540 For example, if certain pathways become up-regulated in response to mild
541 liver stress caused by APAP, then these sensitive parameters may be one of
542 the contributing factors.

543 It can be seen that system operates over a number of distinct timescales.
544 At $t = O(\epsilon) \sim 45$ minutes we see sulphate levels begin to decline in response
545 to the APAP present. As time progresses, we observe that sulphates begin

546 to decline, and by $t = O(1) \sim 8$ hours we see that sulphates have become
547 exhausted as they drop by an order of magnitude (i.e. $S = O(\epsilon)$). At
548 this stage in our analysis, we see a critical divergence between the safe dose
549 and overdose cases at an initial paracetamol dose of 4.54g (using data from
550 Table 2). We also are able to identify timescales for exhaustion and recovery
551 of GSH and sulphates (details of which are available in the supplementary
552 material). Of course there can be considerable individual variability that can
553 affect the critical dose level. The sensitivity analysis has enabled us to deduce
554 that changes in k_G and k_{450} have the largest impact on the dynamics of the
555 system. Further to this, the asymptotic analysis of Section 4 has allowed us
556 to express key quantities (critical concentrations, timescales etc.) in terms
557 of relatively simple formula (Section 4.3), so the effect of varying parameters
558 can be explicitly observed. Such methods have broad application and are
559 somewhat underused in the study of mathematical models in pharmacology.

560 Our parameter selection is good but there are gaps in the current lit-
561 erature that highlight a need for more data on the metabolism of APAP
562 in humans. While literature is available which has allowed us to begin pa-
563 rameterisation, further experimental work would benefit the robustness of
564 the model greatly. The parameter values for glucuronidation and oxida-
565 tion pathways are obtainable from the literature, whilst that of sulphation
566 is less well characterised. Though the analysis in this paper suggests that
567 acetaminophen metabolism via the sulphation pathway is secondary in hu-
568 mans, it appears to be important in rats [12], which are much more resistant

569 to APAP at human toxic levels. Consequently the critical concentration ex-
570 pression, equation (18), will be completely different for rats; we expect that
571 the model is suitably generic to describe acetaminophen metabolism in other
572 species with little modification. However, to fully understand the contrast
573 between rat and human models, for example, more data on metabolism via
574 sulphation and subsequent model reparamaterisation for the different species
575 is essential.

576 Through numerical, sensitivity and asymptotic analysis we have improved
577 our understanding of how the different pathways behave. We have high-
578 lighted key parameters that our system is sensitive to and also found how
579 the pathways interact with each other, and how this affects the production of
580 protein adducts and the potential for toxicity. This work will provide a foun-
581 dation on which to build by working directly with scientific researchers and
582 provides us with new areas to research and expand upon using the existing
583 model.

584 This research is part of a larger project funded by the National Cen-
585 tre for the Replacement, Refinement and Reduction of Animals in Research
586 (NC3R's) which aims to improve *in vitro* testing and reduce the animal test-
587 ing in science [35]. From the initial results and insights, this model is an
588 encouraging first step towards the long-term goal of combining modelling
589 and experimental approaches to mitigate the use of animal testing in toxi-
590 cological studies, for example, testing hypotheses which would normally be
591 tested in animal models. It's simplicity and analytical tractability means

592 that we can draw conclusions on key parameters that can then be found
593 from *in vitro* data.

594 **Competing Interests**

595 We have no competing interests.

596 **Authors' Contributions**

597 DR and JW carried out all numerical and analytical work on the model
598 and drafted this article. JW, DW, SR and SW created the original pathway
599 model well as providing a biological perspective on the work being carried
600 out. All authors assisted in drafting the publication and have given final
601 approval for publication.

602 **Acknowledgments**

603 All authors gratefully acknowledge the National Centre for the Replace-
604 ment, Refinement and Reduction of Animals in Research (NC3R's) for fund-
605 ing support via a PhD studentship and the 2011 CRACK-IT IVIVE challenge
606 award.

607 **Funding**

608 All funding for authors on this work has come from the NC3R's via a stu-
609 dentship (NC/K500422/1) and the 2011 CRACK-IT IVIVE challenge award.

- [1] J. Lazarou, B. H. Pomeranz, P. N. Corey, Incidence of adverse drug reactions in hospitalized patients, *JAMA: the journal of the American Medical Association* 279 (15) (1998) 1200–1205.
- [2] P. Nourjah, S. R. Ahmad, C. Karwoski, M. Willy, Estimates of acetaminophen (paracetamol)-associated overdoses in the united states, *Pharmacoepidemiology and drug safety* 15 (6) (2006) 398–405.
- [3] K. Hawton, H. Bergen, S. Simkin, E. Arensman, P. Corcoran, J. Cooper, K. Waters, D. Gunnell, N. Kapur, Impact of different pack sizes of paracetamol in the united kingdom and ireland on intentional overdoses: a comparative study, *BMC public health* 11 (1) (2011) 460.
- [4] G. Ostapowicz, R. J. Fontana, F. V. Schiødt, A. Larson, T. J. Davern, S. H. Han, T. M. McCashland, A. O. Shakil, J. E. Hay, L. Hynan, et al., Results of a prospective study of acute liver failure at 17 tertiary care centers in the united states, *Annals of internal medicine* 137 (12) (2002) 947–954.
- [5] W. M. Lee, et al., Acute liver failure in the united states, in: *Seminars in liver disease*, Vol. 23, GEORG THIEME VERLAG, 2003, pp. 217–226.
- [6] D. C. Davis, W. Z. Potter, D. J. Jollow, J. R. Mitchell, Species differences in hepatic glutathione depletion, covalent binding and hepatic necrosis after acetaminophen, *Life Sciences* 14 (11) (1974) 2099–2109.

- [7] J. W. Allen, S. R. Khetani, S. N. Bhatia, In vitro zonation and toxicity in a hepatocyte bioreactor, *Toxicological sciences* 84 (1) (2005) 110–119.
- [8] Z. Riches, J. Bloomer, A. Patel, A. Nolan, M. Coughtrie, Assessment of cryopreserved human hepatocytes as a model system to investigate sulfation and glucuronidation and to evaluate inhibitors of drug conjugation, *Xenobiotica* 39 (5) (2009) 374–381.
- [9] A. E. Mutlib, T. C. Goosen, J. N. Bauman, J. A. Williams, S. Kulkarni, S. Kostrubsky, Kinetics of acetaminophen glucuronidation by udp-glucuronosyltransferases 1a1, 1a6, 1a9 and 2b15. potential implications in acetaminophen-induced hepatotoxicity, *Chemical research in toxicology* 19 (5) (2006) 701–709.
- [10] S. X. Duan, L. L. von Moltke, D. J. Greenblatt, C. J. Patten, J. O. Miners, P. I. Mackenzie, et al., Interindividual variability in acetaminophen glucuronidation by human liver microsomes: identification of relevant acetaminophen udp-glucuronosyltransferase isoforms, *Journal of Pharmacology and Experimental Therapeutics* 299 (3) (2001) 998–1006.
- [11] D. J. Sweeny, L. A. Reinke, Sulfation of acetaminophen in isolated rat hepatocytes. relationship to sulfate ion concentrations and intracellular levels of 3'-phosphoadenosine-5'-phosphosulfate., *Drug metabolism and disposition* 16 (5) (1988) 712–715.
- [12] D. Reith, N. J. Medlicott, R. Kumara De Silva, L. Yang, J. Hickling,

- M. Zacharias, Simultaneous modelling of the michaelis-menten kinetics of paracetamol sulphation and glucuronidation, *Clinical and Experimental Pharmacology and Physiology* 36 (1) (2009) 35–42.
- [13] C. J. Patten, P. E. Thomas, R. L. Guy, M. Lee, F. J. Gonzalez, F. P. Guengerich, C. S. Yang, Cytochrome p450 enzymes involved in acetaminophen activation by rat and human liver microsomes and their kinetics, *Chemical research in toxicology* 6 (4) (1993) 511–518.
- [14] W. Chen, L. L. Koenigs, S. J. Thompson, R. M. Peter, A. E. Rettie, W. F. Trager, S. D. Nelson, Oxidation of acetaminophen to its toxic quinone imine and nontoxic catechol metabolites by baculovirus-expressed and purified human cytochromes p450 2e1 and 2a6, *Chemical research in toxicology* 11 (4) (1998) 295–301.
- [15] K. E. Thummel, C. A. Lee, K. L. Kunze, S. D. Nelson, J. T. Slattery, Oxidation of acetaminophen to n-acetyl-p-aminobenzoquinoneimine by human cyp3a4, *Biochemical pharmacology* 45 (8) (1993) 1563–1569.
- [16] J. B. Vaidyanathan, T. Walle, Glucuronidation and sulfation of the tea flavonoid (-)-epicatechin by the human and rat enzymes, *Drug metabolism and disposition* 30 (8) (2002) 897–903.
- [17] C. Guerri, S. Grisolia, Changes in glutathione in acute and chronic alcohol intoxication, *Pharmacology Biochemistry and Behavior* 13 (1980) 53–61.

- [18] D. Wood, D. Wood, P. Dargan, A review of the evidence concerning hepatic glutathione depletion and susceptibility to hepatotoxicity after paracetamol overdose, *Open Access Emergency Medicine* 87.
- [19] J. G. D. Ochoa, J. Bucher, A. R. Péry, J. M. Z. Comenges, J. Niklas, K. Mauch, A multi-scale modeling framework for individualized, spatiotemporal prediction of drug effects and toxicological risk, *Frontiers in pharmacology* 3.
- [20] R. Ben-Shachar, Y. Chen, S. Luo, C. Hartman, M. Reed, H. F. Nijhout, et al., The biochemistry of acetaminophen hepatotoxicity and rescue: a mathematical model, *Theoretical Biology and Medical Modelling* 9 (1) (2012) 55.
- [21] L. Prescott, Kinetics and metabolism of paracetamol and phenacetin., *British Journal of Clinical Pharmacology* 10 (S2) (1980) 291S–298S.
- [22] C. H. Remien, F. R. Adler, L. Waddoups, T. D. Box, N. L. Sussman, Mathematical modeling of liver injury and dysfunction after acetaminophen overdose: early discrimination between survival and death, *Hepatology* 56 (2) (2012) 727–734.
- [23] D. P. Williams, R. Shipley, M. J. Ellis, S. Webb, J. Ward, I. Gardner, S. Creton, Novel in vitro and mathematical models for the prediction of chemical toxicity, *Toxicology Research* 2 (1) (2013) 40–59.

- [24] L. Bilinsky, M. Reed, H. Nijhout, The role of skeletal muscle in liver glutathione metabolism during acetaminophen overdose, *Journal of theoretical biology* 376 (2015) 118–133.
- [25] C. D. Klaassen, S. A. Reisman, Nrf2 the rescue: effects of the antioxidative/electrophilic response on the liver, *Toxicology and applied pharmacology* 244 (1) (2010) 57–65.
- [26] D. G. Craig, C. M. Bates, J. S. Davidson, K. G. Martin, P. C. Hayes, K. J. Simpson, Staggered overdose pattern and delay to hospital presentation are associated with adverse outcomes following paracetamol-induced hepatotoxicity, *British journal of clinical pharmacology* 73 (2) (2012) 285–294.
- [27] M. Ookhtens, K. Hobdy, M. Corvasce, T. Y. Aw, N. Kaplowitz, Sinusoidal efflux of glutathione in the perfused rat liver. evidence for a carrier-mediated process., *Journal of Clinical Investigation* 75 (1) (1985) 258.
- [28] B. H. Lauterburg, J. D. Adams, J. R. Mitchell, Hepatic glutathione homeostasis in the rat: efflux accounts for glutathione turnover, *Hepatology* 4 (4) (1984) 586–590.
- [29] T. Aw, M. Ookhtens, C. Ren, N. Kaplowitz, Kinetics of glutathione efflux from isolated rat hepatocytes, *Am. J. Physiol* 250 (1986) G236–G243.

- [30] D. J. Miner, P. T. Kissinger, Evidence for the involvement of n-acetyl-p-benzoquinone imine in acetaminophen metabolism, *Biochemical pharmacology* 28 (22) (1979) 3285–3290.
- [31] A. Saltelli, *Global Sensitivity Analysis: The Primer*, John Wiley & Sons, Ltd, West Sussex, UK, 2008.
- [32] E. A. Carter, Enhanced acetaminophen toxicity associated with prior alcohol consumption in mice: prevention by n-acetylcysteine, *Alcohol* 4 (1) (1987) 69–71.
- [33] C. A. Lee, J. H. Lillibridge, S. D. Nelson, J. T. Slattery, Effects of caffeine and theophylline on acetaminophen pharmacokinetics: P450 inhibition and activation., *Journal of Pharmacology and Experimental Therapeutics* 277 (1) (1996) 287–291.
- [34] G. P. Bray, P. M. Harrison, J. G. O’Grady, J. M. Tredger, R. Williams, Long-term anticonvulsant therapy worsens outcome in paracetamol-induced fulminant hepatic failure, *Human & experimental toxicology* 11 (4) (1992) 265–270.
- [35] D. Krewski, D. Acosta Jr, M. Andersen, H. Anderson, J. C. Bailar III, K. Boekelheide, R. Brent, G. Charnley, V. G. Cheung, S. Green Jr, et al., Toxicity testing in the 21st century: a vision and a strategy, *Journal of Toxicology and Environmental Health, Part B* 13 (2-4) (2010) 51–138.

- [36] U. Frevort, S. Engelmann, S. Zougbedé, J. Stange, B. Ng, K. Matuschewski, L. Liebes, H. Yee, Intravital observation of plasmodium berghei sporozoite infection of the liver, PLoS biology 3 (6) (2005) e192.